J|A|C|S ARTICLES

Published on Web 02/13/2009

Structural Evolution of Doped Gold Clusters: MAu_x^- (M = Si, Ge, Sn; $x = 5-8$)

Rhitankar Pal,[†] Lei-Ming Wang,[‡] Wei Huang,[‡] Lai-Sheng Wang,*[,‡] and Xiao Cheng Zeng*[,†]

Department of Chemistry, University of Nebraska-Lincoln, Lincoln, Nebraska 68588, Department of Physics, Washington State University, 2710 University Drive, Richland, Washington 99354, and Chemical & Materials Sciences Division, Pacific Northwest National Laboratory, MS K8-88, P.O. Box 999, Richland, Washington 99352

Received December 31, 2008; E-mail: ls.wang@pnl.gov; xczeng@phase2.unl.edu

Abstract: We report a joint experimental and theoretical study on the structures of a series of gold clusters doped with a group-14 atom: MAu_x^- (M = Si, Ge, Sn; $x = 5-8$). Well-resolved photoelectron spectra were obtained and compared to calculations at several levels of theory to identify the low-lying structures of MAu_{5-8}^-. We found that the structure of $SiAu_5^-$ is dominated by the tetrahedrally coordinated Si motif, which can be viewed as built from the tetrahedral $SiAu_4^-$ by an extra Au atom bonded to a terminal gold atom. However, $SiAu_6^-$ and $SiAu_7^-$ have quasi-planar structures, similar to those of $GeAu_6^-$/$SnAu_6^-$ and $GeAu_7^-$/$SnAu_7^-$, respectively. $SiAu_8^-$ again has a tetrahedrally coordinated Si structure, which displays a structural motif of a dangling Au−Si unit sitting on a gold cluster surface, resembling that of the larger Si-doped gold cluster $SiAu_{16}^-$. For M = Ge, Sn, our results show that the major isomers of $GeAu_{5-8}^-$ have structures similar to those of the corresponding $SnAu_{5-8}^-$ clusters, and they can be viewed as grown from the previously suggested square-pyramidal $GeAu_4^-$ and $SnAu_4^-$, respectively. Population of minor isomers was observed for $SnAu_5^-$, $GeAu_6^-$, $SnAu_6^-$, and $GeAu_8^-$. The 3D to quasi-2D to 3D structural evolution for $SiAu_5^-$ to $SiAu_8^-$ and the *structural convergence* for MAu_x^- (M = Si, Ge, Sn) at $x = 6$, 7 manifest competitions between the tendency of forming molecule-like structures around the group-14 dopant (optimizing M−Au interactions) and the strong tendency of forming planar structures for small gold anion clusters (optimizing Au−Au interactions).

1. Introduction

Since the discovery of unusual catalytic capabilities of gold nanoclusters,[1] considerable attention has been devoted to resolving structures of gold nanoclusters from bottom up.[2] Structures of bare gold clusters in the small-to-medium size range have been determined through joint experimental and theoretical studies.[3−16] To date, it is known that small-sized anion gold clusters Au_4^- to Au_{12}^- exhibit 2D planar structures,[3−5] Au_{16}^- to Au_{18}^- possess hollow-cage structures,[6,7] and both anion and neutral Au_{20}^- and Au_{20} have the tetrahedral structure (the smallest gold pyramid).[8] For medium-sized gold clusters, Au_{24}^- possibly possesses tubular structure,[9,10] and Au_{25}^-,[10] Au_{32}^-,[11,12] Au_{34}^-,[13] and Au_{55}^- to Au_{64}^- [14−16] all exhibit core−shell structures.

It has also been demonstrated that doped gold clusters with an impurity atom can show distinctive structures and interesting properties. For example, doping a W atom in Au_{12}^- cluster results in an endohedral cluster with icosahedral symmetry, I_h-W@Au_{12}^-.[17,18] Similarly, a V (or Nb, Ta) atom can also

[†] University of Nebraska-Lincoln.
[‡] Washington State University and Pacific Northwest National Laboratory.

(1) Haruta, M. *Catal. Today* **1997**, *36*, 153.
(2) (a) Pyykkö, P. *Angew. Chem., Int. Ed.* **2004**, *43*, 4412. (b) Herzing, A. A.; Kiely, C. J.; Carley, A. F.; Landon, P.; Hutchings, G. J. *Science* **2008**, *321*, 1331.
(3) Häkkinen, H.; Moseler, M.; Landman, U. *Phys. Rev. Lett.* **2002**, *89*, 033401.
(4) Furche, F.; Ahlrichs, R.; Weis, P.; Jacob, C.; Glib, S.; Bierweiler, T.; Kappes, M. M. *J. Chem. Phys.* **2002**, *117*, 6982.
(5) Häkkinen, H.; Yoo, B.; Landman, U.; Li, X.; Zhai, H. J.; Wang, L. S. *J. Phys. Chem. A* **2003**, *107*, 6168.
(6) Bulusu, S.; Li, X.; Wang, L. S.; Zeng, X. C. *Proc. Natl. Acad. Sci. U.S.A.* **2006**, *103*, 8326.
(7) Xing, X.; Yoon, B.; Landman, U.; Parks, J. H. *Phys. Rev. B* **2006**, *74*, 165423.
(8) (a) Li, J.; Li, X.; Zhai, H.-J.; Wang, L. S. *Science* **2003**, *299*, 864. (b) Gruene, P.; Rayner, D. M.; Redlich, B.; van der Meer, A. F. G.; Lyon, G. T.; Meijer, G.; Fielicke, A. *Science* **2008**, *321*, 674.
(9) Yoon, B.; Koskinen, P.; Huber, B.; Kostko, B.; v. Issendorff, B.; Häkkinen, H.; Moseler, M.; Landman, U. *ChemPhysChem.* **2007**, *8*, 157.
(10) Bulusu, S.; Li, X.; Wang, L. S.; Zeng, X. C. *J. Phys. Chem. C* **2007**, *111*, 4190.
(11) Ji, M.; Gu, X.; Li, X.; Gong, X.; Li, J.; Wang, L. S. *Angew. Chem., Int. Ed.* **2005**, *44*, 7119.
(12) Jalbout, A. F.; Contreras-Torres, F. F.; Perez, L. A.; Garzon, I. L. *J. Phys. Chem. C* **2008**, *112*, 353.
(13) (a) Lechtken, A.; Schooss, D.; Stairs, J. R.; Blom, M. N.; Furche, F.; Morgner, N.; Kostko, O.; von Issendorff, B.; Kappes, M. M. *Angew. Chem., Int. Ed.* **2007**, *46*, 2944. (b) Gu, X.; Bulusu, S.; Li, X.; Zeng, X.-C.; Li, J.; Gong, X.-G.; Wang, L. S. *J. Phys. Chem. C* **2007**, *111*, 8228. (c) Santizo, I. E.; Hidalgo, F.; Perez, L. A.; Noguez, C.; Garzon, I. L. *J. Phys. Chem. C* **2008**, *112*, 17533.
(14) Garzon, I. L.; Michaelian, K.; Beltran, M. R.; Posada-Amarillas, A.; Ordejon, P.; Artacho, E.; Sanchez-Portal, D.; Soler, J. M. *Phys. Rev. Lett.* **1998**, *81*, 1600.
(15) Häkkinen, H.; Moseler, M.; Kostko, O.; Morgner, N.; Hoffmann, M. A.; v. Issendorff, B. *Phys. Rev. Lett.* **2004**, *93*, 093401.
(16) Huang, W.; Ji, M.; Dong, C.-D.; Gu, X.; Wang, L.-M.; Gong, X. G.; Wang, L. S. *ACS Nano* **2008**, *2*, 897.

 10.1021/ja810093t CCC: $40.75

strongly affect the structure of bare Au_{12}^- cluster to form the endohedral structure I_h-V@Au_{12}^-.[19] Previous theoretical studies predicted that Au_{14} doped with an early transition-metal atom Sc, Y, Zr, or Hf can form endohedral clusters with large highest occupied molecular orbital (HOMO)−lowest unoccupied molecular orbital (LUMO) gaps.[20] A series of transition-metal atom doped gold clusters have been studied through photofragmentation experiment.[21,22] As the size of gold clusters increases, it is expected that the effect of a dopant atom on the overall structure of doped gold clusters diminishes. Indeed, our recent study shows that doping the hollow golden cage Au_{16}^- with a Cu atom (or a Ag atom) results in the endohedral cluster Cu@Au_{16}^- (or Ag@Au_{16}^-) with little structural deformation to the original golden cage.[23]

There have been relatively few studies on gold clusters doped with group-14 atoms.[24−29] One of the most intriguing findings is the Au/H analogy first discovered in the tetrahedral $SiAu_4^{-1/0}$ cluster,[24a] and later confirmed and extended in other small Si-doped gold clusters, such as $Si_2Au_4^{-1/0}$, $Si_2Au_2^{-1/0}$, and $Si_3Au_3^{-1/0/+1}$.[24b,c] On the other hand, doping Si into the golden cage cluster Au_{16}^- leads to an exohedral structure of Au−$SiAu_{15}^-$ where a Au atom is relocated from the original golden cage to form a dangling Au−Si unit on the Si atom.[28] This intriguing exohedral structure of $SiAu_{16}^-$ reflects an interplay between the tendency of forming the tetrahedral $SiAu_4$ local unit and the tendency to retain overall structural integrity for the growing gold clusters. Moving down group-14 in the periodic table, it has been shown that Ge or Sn doping can affect structures of gold clusters in different ways than the Si dopant. For example, ab initio computation suggests that the Au/H analogy does not exist in $GeAu_4^-$ and $SnAu_4^-$, and these two clusters exhibit square-pyramidal C_{4v} structures,[25b] rather than the T_d structure of $SiAu_4^-$.[24a] Moreover, doping a Ge or Sn atom into Au_{16}^- cluster gives rise to an exohedral structure for $GeAu_{16}^-$ or $SnAu_{16}^-$ without showing a Au−Ge or Au−Sn dangling unit as observed in $SiAu_{16}^-$.[28b] The structural differences between Si- and Ge/Sn-doped gold clusters can be attributed to the fact that Si has stronger tendency to form directional bonding using sp^3 hybridization than Ge and Sn.

To date, two types of structures of group-14 atom-doped gold anion clusters have been shown: (1) the molecular-like structures of small $Si_xAu_y^-$ clusters ($x = 1-3$, $y = 1-4$),[24,25] and (2) the "clusterlike" cage structures of MAu_{16}^- (M = Si, Ge, Sn).[28] In this joint experimental and theoretical study, we explore the structural evolution of Si-, Ge-, and Sn-doped anion Au clusters, MAu_x^- (M = Si, Ge, Sn), in the size range of $x = 5-8$. We focus on (1) the structural evolution and the interplay between molecule-like behavior around the group-14 dopant (e.g., local T_d $SiAu_4$ unit) and the tendency to retain overall structural integrity of the gold clusters with increasing cluster size (e.g., in $SiAu_{16}^-$), and (2) how the chemical similarity and/or difference among Si, Ge, and Sn dopant affect the growth pattern of Si-, Ge-, and Sn-doped Au clusters.

2. Experimental Methods

The experiments were performed on a magnetic bottle photoelectron spectroscopy (PES) apparatus equipped with a laser vaporization supersonic cluster source, details of which were described elsewhere.[30] Briefly, the doped gold clusters were produced by laser vaporization of a Au/Si, Au/Ge, or Au/Sn composite disk target containing about 2% Si, 2% Ge, or 2.5% Sn, respectively, with a helium carrier gas. Anion clusters were extracted from the cluster beam perpendicularly and analyzed using a time-of-flight mass spectrometer. The clusters of interest were mass-selected and decelerated before being photodetached by a 193-nm laser beam from an ArF excimer laser. Photoelectrons were guided toward the detector by the magnetic bottle at nearly 100% collecting efficiency and analyzed by the time-of-flight electron energy analyzer. The spectra were calibrated using the known spectra of Au^-. The PES apparatus had an energy resolution of $\Delta E/E \approx 2.5\%$ (i.e., about 25 meV for 1 eV kinetic energy electrons).

3. Computational Methods

To search for low-lying structures of MAu_{5-8}^- (M = Si, Ge, Sn), we employed the basin-hopping global optimization technique coupled with the density functional theory (DFT) for geometry optimization.[31,32] Generalized gradient approximation in the Perdue−Burke−Ernzerhof (PBE)[33] functional form was chosen. Several randomly selected initial structures were used for the basin-hopping searches, all leading to consistent sets of low-lying isomers for each species (Figures S1−S4 in the Supporting Information, and Tables 2−5). These low-lying isomers were reoptimized using the PBE functional (PBEPBE key word) with a scalar relativistic effective core potential Stuttgart/Dresden (SDD) basis set,[34] implemented in the Gaussian03 (G03) package.[35] Harmonic vibrational frequencies were computed to confirm that the low-energy isomers are true minima (Tables S1−S4 in the Supporting Information). The relative energies of the top-5 isomers were further examined using the PBE/TZP functional/basis set, implemented in the ADF software package.[36] If the two independent DFT calculations give rise to inconsistent energy rankings among leading isomers, higher-level ab initio calculations were further carried out

(17) Pyykkö, P.; Runeberg, N. *Angew. Chem., Int. Ed.* **2002**, *41*, 2174.
(18) Li, X.; Kiran, B.; Li, J.; Zhai, H. J.; Wang, L. S. *Angew. Chem., Int. Ed.* **2002**, *41*, 4786.
(19) Zhai, H. J.; Li, J.; Wang, L. S. *J. Chem. Phys.* **2004**, *121*, 8369.
(20) (a) Gao, Y.; Bulusu, S.; Zeng, X. C. *J. Am. Chem. Soc.* **2005**, *127*, 15680. (b) Gao, Y.; Bulusu, S.; Zeng, X. C. *ChemPhysChem* **2006**, *7*, 2275.
(21) Neukermans, S.; Janssens, E.; Tanaka, H.; Silverans, R. E.; Lievens, P. *Phys. Rev. Lett.* **2003**, *90*, 033401.
(22) Janssens, E.; Tanaka, H.; Neukermans, S.; Silverans, R. E.; Lievens, P. *Phys. Rev. B* **2004**, *69*, 085402.
(23) (a) Wang, L. M.; Bulusu, S.; Zhai, H. J.; Zeng, X. C.; Wang, L. S. *Angew. Chem., Int. Ed.* **2007**, *46*, 2915. (b) Wang, L. M.; Pal, R.; Huang, W.; Zeng, X. C.; Wang, L. S. *J. Chem. Phys.* **2009**, *130*, 051101.
(24) (a) Kiran, B.; Li, X.; Zhai, H.-J.; Cui, L. F.; Wang, L. S. *Angew. Chem., Int. Ed.* **2004**, *43*, 2125. (b) Li, X.; Kiran, B.; Wang, L. S. *J. Phys. Chem. A* **2005**, *109*, 4366. (c) Kiran, B.; Li, X.; Zhai, H.-J.; Wang, L. S. *J. Chem. Phys.* **2006**, *125*, 133204.
(25) (a) Pyykkö, P.; Zhao, Y. *Chem. Phys. Lett.* **1991**, *177*, 103. (b) Pal, R.; Bulusu, S.; Zeng, X. C. *J. Comput. Methods Sci. Eng.* **2007**, *7*, 185.
(26) (a) Majumder, C.; Kandalam, A. K.; Jena, P. *Phys. Rev. B* **2006**, *74*, 205437. (b) Majumder, C. *Phys. Rev. B* **2007**, *75*, 235409.
(27) (a) Walter, M.; Häkkinen, H. *Phys. Chem. Chem. Phys.* **2006**, *8*, 5407.
(28) (a) Sun, Q.; Wang, Q.; Chen, G.; Jena, P. *J. Chem. Phys.* **2007**, *127*, 214706. (b) Wang, L.-M.; Bulusu, S.; Huang, W.; Pal, R.; Wang, L. S.; Zeng, X. C. *J. Am. Chem. Soc.* **2007**, *129*, 15136.
(29) Abe, M.; Nakajima, T.; Hirao, K. *J. Chem. Phys.* **2002**, *117*, 7960.
(30) (a) Wang, L. S.; Cheng, H. S.; Fan, J. *J. Chem. Phys.* **1995**, *102*, 9480. (b) Wang, L. S.; Wu, H. In *Cluster Materials*; Duncan, M. A., Ed.; Advances in Metal and Semiconductor Clusters IV; JAI Press: Greenwich, CT, 1998; pp 299−343.
(31) (a) Wales, D. J.; Scheraga, H. A. *Science* **1999**, *285*, 1368. (b) Yoo, S.; Zeng, X. C. *J. Chem. Phys.* **2003**, *119*, 1442. (c) Yoo, S.; Zeng, X. C. *Angew. Chem., Int. Ed.* **2005**, *44*, 1491.
(32) Delley, B. *J. Chem. Phys.* **1990**, *92*, 508. DMol^3 is available from Accelrys.
(33) Perdew, J. P.; Burke, K.; Ernzerhof, M. *Phys. Rev. Lett.* **1996**, *77*, 3865.
(34) Dolg, M.; Wedig, U.; Stoll, H.; Preuss, H. *J. Chem. Phys.* **1987**, *86*, 866.
(35) Frisch, M. J.; et al. Gaussian 03, revision C.02; Gaussian, Inc.: Wallingford, CT, 2004.

Table 1. Experimentally Observed ADEs and VDEs from Anion Photoelectron Spectra of MAu_{5-8}^- (M = Si, Ge, Sn)[a]

species		ADE (eV)	VDE (eV) X	A	B	C	D	E	F
MAu_5^-	$SiAu_5^-$	4.11 (6)	4.21 (3)	~4.6	5.35 (6)				
	$GeAu_5^-$	3.62 (6)	3.68 (4)	3.94(4)	4.72 (4)				
	$SnAu_5^-$	3.53 (5)	3.58 (4)	3.85(4)	4.70 (4)				
MAu_6^-	$SiAu_6^-$	2.62 (5)	2.70 (3)	3.67(3)	3.97 (3)				
	$GeAu_6^-$	2.59 (6)	2.65 (4)	3.58(4)	3.90 (4)				
	$SnAu_6^-$	2.53 (6)	2.57 (4)	3.52(4)	3.82 (4)				
MAu_7^-	$SiAu_7^-$	3.35 (5)	3.40 (3)	4.29(3)	4.41 (2)	4.98 (3)			
	$GeAu_7^-$	3.35 (6)	3.38 (4)	4.24(4)	4.71 (4)	4.94 (3)			
	$SnAu_7^-$	3.28 (6)	3.30 (4)	4.12(4)	4.74 (3)	4.87 (3)			
MAu_8^-	$SiAu_8^-$	3.14 (5)	3.23 (3)	3.98(2)	4.13 (2)	4.31 (2)	4.48 (2)	4.77 (2)	4.95 (3)
	$GeAu_8^-$	2.69 (6)	2.73 (4)	4.11(4)	4.25 (4)				
	$SnAu_8^-$	2.68 (6)	2.74 (4)	4.11(3)	4.28 (4)	4.50 (4)			

[a] The numbers in parentheses indicate the uncertainties in the last digit.

Table 2. Relative Energies of Five Low-Lying Isomers of MAu_5^- (M = Si, Ge, Sn) at PBE/TZP (ADF) and PBEPBE/SDD (G03) Levels of Theory, as well as MP2/aug-cc-pVDZ//MP2/SDD, MP4(SDQ)/aug-cc-pVDZ//MP2/SDD, CCSD(T)/aug-cc-pVDZ//MP2/SDD Levels of Theory for $SiAu_5^-$, MP2/aug-cc-pVDZ//MP2/SDD, and MP4(SDQ)/aug-cc-pVDZ//MP2/SDD Levels of Theory for $GeAu_5^-$, and MP2/SDD and MP4(SDQ)/SDD//MP2/SDD Levels of Theory for $SnAu_5^-$[a]

isomer		relative energies (eV) ADF	G03	MP2	MP4(SDQ)	CCSD(T)	VDE (eV) ADF	exptl
$SiAu_5^-$	1	**0.000**	**0.000**	0.244	**0.000**	**0.000**	3.86	4.21 (3)
	2	0.466	0.199	**0.000**	0.024	0.139	3.86	
	3	0.273	0.093	0.154	0.083	0.148	3.70	
	4	0.415	0.165	0.114	0.068	0.182	3.59	
	5	0.377	0.363	0.668	0.277		3.23	
$GeAu_5^-$	1	**0.000**	0.003	0.064	**0.000**		3.43	3.68 (4)
	2	0.045	0.066	**0.000**	0.003		3.99	
	3	0.006	**0.000**	0.143	0.108		3.57	
	4	0.301	0.282				3.18	
	5	0.322	0.255				4.27	
$SnAu_5^-$	1	**0.000**	0.023	**0.000**	**0.000**		3.38	3.58 (4)
	2	0.046	0.093	0.092	0.092		3.90	
	3	0.027	**0.000**	0.195	0.196		3.68	
	4	0.214	0.272	0.209			3.07	
	5	0.311	0.381	0.210			2.67	

[a] Top-3 (or top-5) isomers are ranked according to their relative energies at either the CCSD(T) or MP4(SDQ) level, and the remaining isomers are ranked on the basis of MP2 or PBE/TZP level. The VDEs are computed at PBE/TZP (ADF) level of theory and compared to the experimental values. Energies of the lowest-energy isomers are highlighted in bold.

Table 3. Relative Energies of Five Low-Lying Isomers of MAu_6^- (M = Si, Ge, Sn) at PBE/TZP (ADF) and PBEPBE/SDD (G03) Levels of Theory, as well as MP2/aug-cc-pVDZ//MP2/SDD and MP4(SDQ)/aug-cc-pVDZ//MP2/SDD Levels of Theory for $SiAu_6^-$ and $GeAu_6^-$, and MP2/SDD and MP4(SDQ)/SDD//MP2/SDD Levels of Theory for $SnAu_6^-$[a]

isomer		relative energies (eV) ADF	G03	MP2	MP4(SDQ)	VDE (eV) ADF	exptl
$SiAu_6^-$	1	0.121	0.006	**0.000**	**0.000**	2.62	2.70 (3)
	2	0.088	**0.000**	0.067	0.045	2.75	
	3	**0.000**	0.125	0.584	0.309	2.63	
	4	0.082	0.171			3.37	
	5	0.115	0.195			2.96	
$GeAu_6^-$	1	**0.000**	**0.000**	**0.000**	**0.000**	2.58	2.65 (4)
	2	0.050	0.055	0.261	0.033	2.84	
	3	0.126	0.118	0.191	0.147	3.00	
	4	0.136	0.110			2.29	
	5	0.144	0.141			2.81	
$SnAu_6^-$	1	0.009	0.056	0.156	**0.000**	2.75	2.57 (4)
	2	**0.000**	0.007	**0.000**	0.075	2.54	
	3	0.032	**0.000**	0.170	0.281	2.33	
	4	0.116	0.131			2.90	
	5	0.118	0.114			2.99	

[a] Top-3 isomers are ranked according to their relative energies at the MP4(SDQ) level, and the remaining isomers are ranked on the basis of PBE/TZP level of theory. The VDEs are computed at PBE/TZP (ADF) level of theory and compared to the experimental values. Energies of the lowest-energy isomers are highlighted in bold.

to aid structural assignment, which include geometry optimization at the second-order Moller−Plesset perturbation (MP2) level of theory with the SDD basis set[34,37] and the single-point energies at the fourth-order Moller−Plesset perturbation for single, double, and quadruple substitutions [MP4(SDQ)] level with the pseudo-potential coupling Dunning's augmented correlation-consistent aug-cc-pVDZ basis set.[38,39] For $SiAu_5^-$, the single-point energies at the couple-cluster level of theory with singles and doubles with perturbative triples [CCSD(T)] were also used to confirm energy ranking of the low-lying isomers obtained at the MP4(SDQ) level of theory.

To compare with the measured PES spectra, the first vertical detachment energies (VDE) of anion clusters were computed (at PBE/TZP level of theory). The binding energies of deeper orbitals were then added to the first VDE to give VDEs to the excited states. Each VDE was fitted with a Gaussian of width 0.06 eV to yield the simulated PES spectra.

4. Experimental Results

The measured photoelectron spectra of MAu_{5-8}^- (M = Si, Ge, Sn) at 193 nm are displayed in Figures 1−4, respectively, along with the simulated spectra for each species. The VDEs of the labeled detachment bands are given in Table 1. The adiabatic detachment energies (ADE), which also represent the electron affinity of the corresponding neutral MAu_{5-8} clusters, are estimated by drawing a straight line along the rising edge of band X and then adding the instrumental resolution to its intersection with the binding energy axis. The obtained ADEs for MAu_{5-8}^- are also given in Table 1.

4.1. MAu_5^-. As seen in Figure 1, the spectrum of $SiAu_5^-$ is relatively simple with four apparent features (Figure 1a). The X band is sharp and intense, which defines an accurate VDE of 4.21 eV. The A and B bands are rather broad with some unresolved features, suggesting that they likely contain multiple

(36) ADF 2008.01; Vrije Universiteit: Amsterdam, 2008. http://www.scm.com.
(37) (a) Schwerdtfeger, P.; Dolg, M.; Schwarz, W. H. E.; Bowmaker, G. A.; Boyd, P. D. W. *J. Chem. Phys.* **1989**, *91*, 1762. (b) Schwerdtfeger, P.; Brown, J. R.; Laerdahl, J. K.; Stoll, H. *J. Chem. Phys.* **2000**, *113*, 7110.
(38) Figgen, D.; Rauhut, G.; Dolg, M.; Stoll, H. *Chem. Phys.* **2005**, *311*, 227.
(39) Peterson, K. A.; Puzzarini, C. *Theor. Chem. Acc.* **2005**, *114*, 283.

Table 4. Relative Energies of Five Low-Lying Isomers of MAu_7^- (M = Si, Ge, Sn) at PBE/TZP (ADF), PBEPBE/SDD (G03), MP2/SDD, and MP4(SDQ)/SDD//MP2/SDD Levels of Theory[a]

		relative energies (eV)				VDE (eV)	
isomer		ADF	G03	MP2	MP4(SDQ)	ADF	exptl
$SiAu_7^-$	1	0.139	**0.000**	**0.000**	**0.000**	3.34	3.40 (3)
	2	0.155	0.029	0.135	0.118	3.43	
	3	**0.000**	0.136	0.925	0.644	3.56	
	4	0.251	0.203			3.36	
	5	0.351	0.278			3.47	
$GeAu_7^-$	1	**0.000**	**0.000**	**0.000**		3.32	3.38 (4)
	2	0.112	0.097	0.212		3.32	
	3	0.110	0.106	0.430		3.55	
	4	0.326	0.302			3.28	
	5	0.350	0.349			3.37	
$SnAu_7^-$	1	0.021	0.059	**0.000**	**0.000**	3.30	3.30 (4)
	2	**0.000**	**0.000**	0.290	0.223	3.29	
	3	0.230	0.223			3.32	
	4	0.334	0.399			3.70	
	5	0.391	0.419			3.58	

[a] Top-2 (or top-3) isomers are ranked according to their relative energies at the MP2 level, and the rest of the isomers are ranked on the basis of PBE/TZP level of theory. The VDEs are computed at PBE/TZP level of theory and compared to the experimental values. Energies of the lowest-energy isomers are highlighted in bold.

Table 5. Relative Energies of Five Low-Lying Isomers of MAu_8^- (M = Si, Ge, Sn) at PBE/TZP (ADF), PBEPBE/SDD (G03), and MP2/SDD Levels of Theory[a]

		relative energies (eV)			VDE (eV)	
isomer		ADF	G03	MP2	ADF	exptl
$SiAu_8^-$	1	**0.000**	**0.000**		3.12	3.23 (3)
	2	0.189	0.160		3.11	
	3	0.190	0.399		2.59	
	4	0.220	0.354		2.48	
	5	0.226	0.334		3.16	
$GeAu_8^-$	1	**0.000**	0.020	**0.000**	2.72	2.73 (4)
	2	0.007	**0.000**	0.216	2.77	
	3	0.152	0.164	0.272	3.17	
	4	0.153	0.133	0.351	2.66	
	5	0.216	0.217		3.15	
$SnAu_8^-$	1	**0.000**	**0.000**		2.76	2.74 (4)
	2	0.179	0.177		2.63	
	3	0.179	0.178		2.93	
	4	0.203	0.196		2.86	
	5	0.244	0.227		2.54	

[a] Isomers are ranked according to their relative energies at the PBE/TZP level of theory. The VDEs are computed at PBE/TZP level of theory and compared to the experimental values. Energies of the lowest-energy isomers are highlighted in bold.

electronic transitions. We note that the patterns of the broad features A and B in the spectrum of $SiAu_5^-$ are similar to the corresponding parts in the spectrum of $SiAu_4^-$,[24a] suggesting that its electronic structure is not significantly altered relative to that of $SiAu_4^-$. Hence, it is possible that their geometrical structures also do not differ too much and the tetrahedral $SiAu_4$ unit[24a] may be retained in $SiAu_5^-$. It was shown previously that $SiAu_4$ is closed shell with a very large gap between its HOMO and its LUMO. In $SiAu_4^-$, the extra electron occupies the delocalized LUMO orbital of $SiAu_4$, giving rise to a very low binding energy peak (X) in its PES spectrum.[24a] In contrast, the first band (X) in $SiAu_5^-$ is at much higher binding energy than that of $SiAu_4^-$, suggesting that it is likely originated from the extra Au atom.

The spectra of $GeAu_5^-$ and $SnAu_5^-$ are very similar (Figure 1b,c), both featuring two closely spaced peaks at ~3.5−4 eV

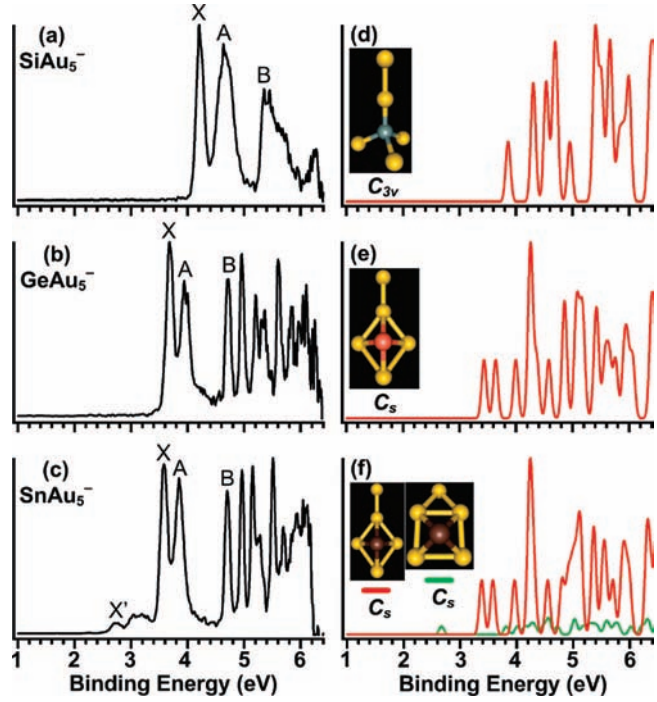

Figure 1. Experimental (left) and simulated (right) photoelectron spectra of MAu_5^- (M = Si, Ge, Sn). The insets show the corresponding structures. The dopant atoms are shown in color (Si in gray, Ge in red, and Sn in brown).

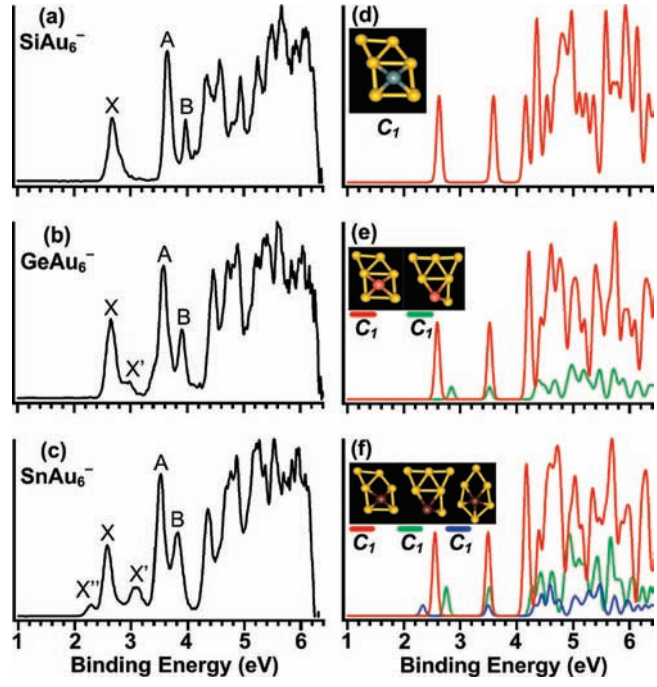

Figure 2. Experimental (left) and simulated (right) photoelectron spectra of MAu_6^- (M = Si, Ge, Sn). The insets show the corresponding structures. The dopant atoms are shown in color (Si in gray, Ge in red, and Sn in brown).

(X and A) followed by a sizable energy gap and several well-resolved peaks. The first VDEs of $GeAu_5^-$ and $SnAu_5^-$ are measured to be 3.68 and 3.58 eV, respectively, notably smaller than that of $SiAu_5^-$ (Table 1). The clear similarities in their PES spectra suggest that $GeAu_5^-$ and $SnAu_5^-$ should have similar structures. However, there are some weak features observed in the spectrum of $SnAu_5^-$ at the low binding energy

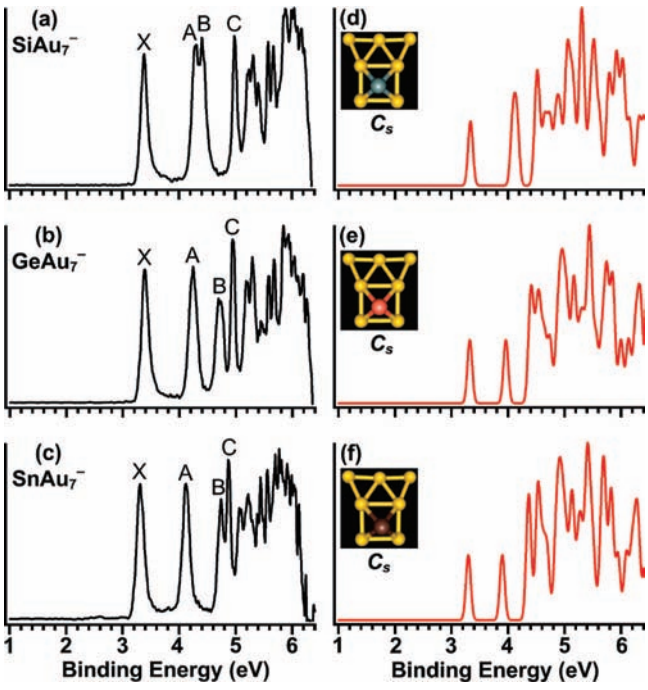

Figure 3. Experimental (left) and simulated (right) photoelectron spectra of MAu_7^- (M = Si, Ge, Sn). The insets show the corresponding structures. The dopant atoms are shown in color (Si in gray, Ge in red, and Sn in brown).

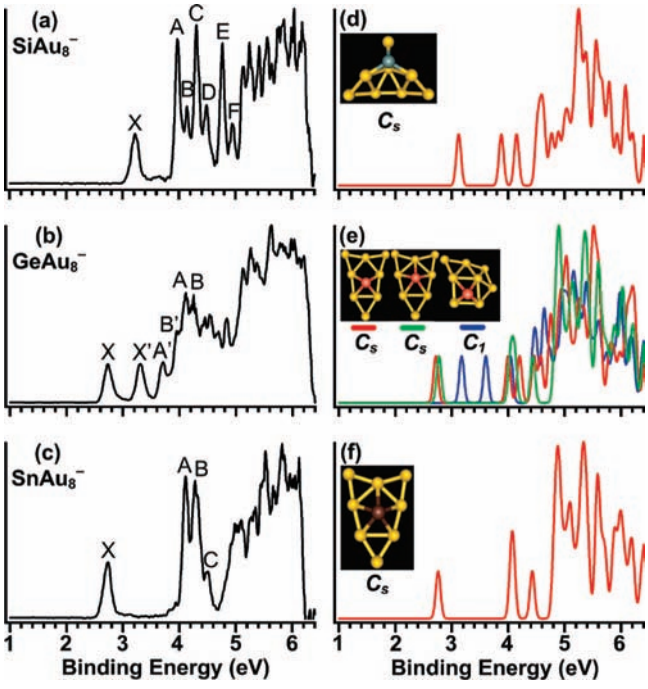

Figure 4. Experimental (left) and simulated (right) photoelectron spectra of MAu_8^- (M = Si, Ge, Sn). The insets show the corresponding structures. The dopant atoms are shown in color (Si in gray, Ge in red, and Sn in brown).

part below ~3.5 eV (Figure 1c), suggesting possible isomers or impurities in the $SnAu_5^-$ cluster beam.

4.2. MAu_6^-. As shown in Figure 2a−c, the overall spectral patterns are similar among the three doped clusters MAu_6^- (M = Si, Ge, Sn), each displaying three peaks in the low binding energy region (<~4 eV) with a fairly large HOMO−LUMO gap (X−A separation): 0.97, 0.93, and 0.95 eV for M = Si, Ge, and Sn, respectively. The first VDEs measured for MAu_6^- are 2.70, 2.65, and 2.57 eV for M = Si, Ge, and Sn, respectively, quite close to each other. The similar doublet features A and B in the spectra of MAu_6^- are likely due to the detachment transitions to the first triplet and singlet excited states of the neutrals, judging by their relative intensities. Since the MAu_6^- anion clusters are open shell with one unpaired electron, detaching one electron from an orbital other than its SOMO (the X band) will result in an excited state of the neutral which could be of either a singlet- or a triplet-spin arrangement. The higher intensity A band represents the detachment transition to the lowest triplet excited state of the neutral MAu_6 species and B the corresponding singlet state. The triplet−singlet splitting (A−B separation) is nearly identical in the three spectra of MAu_6^-: 0.30, 0.32, and 0.30 eV for M = Si, Ge, and Sn, respectively. The spectral similarities as well as their close VDEs, HOMO−LUMO gaps, and possible triplet−singlet splitting suggest that major isomers of MAu_6^- may have similar structures. Again, some weak features are observed in the spectra of $GeAu_6^-$ (X′ in Figure 2b) and $SnAu_6^-$ (X′ and X″ in Figure 2c), indicating the presence of minor isomers.

4.3. MAu_7^-. The spectra of MAu_7^- (Figure 3a−c) are also quite similar to each other, each revealing four well-resolved peaks in the region between 3 and 5 eV followed by more congested bands in the higher binding energy side. The intense and sharp ground-state transition (X) suggests that the MAu_7^- anions are closed shell and there is negligible geometrical change between the anion and the neutral. The binding energies of bands X, A, and C (Table 1) and the overall spectral patterns are very similar for the three MAu_7^- clusters, and even the features beyond 5 eV are also comparable, suggesting that the three clusters should have similar structures. The only major difference among the three spectra is that the binding energy of the B band in the spectrum of $SiAu_7^-$ is much lower as compared to that of $GeAu_7^-$ and $SnAu_7^-$ (Figure 3 and Table 1), suggesting that it is likely due to detachment from a dopant-dominated molecular orbital and reflecting the chemical difference between Si and Ge/Sn in the doped clusters. It should also be noted that the spectra of all three MAu_7^- clusters seem free of weak features due to minor isomers. This implies that there must be a relatively stable structure type for the three clusters.

4.4. MAu_8^-. For MAu_8^-, the three doped clusters display dramatically different PES spectra (Figure 4a−c), suggesting a major structural divergence among them. For $SiAu_8^-$, the first VDE (X) is observed to be 3.23 eV. Following the X band and a HOMO−LUMO gap of 0.75 eV, three sharp excited-state transition bands (A, C, and E, Figure 4a) are observed between ~4 and 5 eV, each followed by a weaker peak with separations of 0.15 eV (A−B), 0.17 eV (C−D), and 0.18 eV (E−F). The relative intensities of these peaks also imply that they are due to transitions to triplet and singlet final states, that is, bands A, C, and E define the first, second, and third triplet excited states of the neutral $SiAu_8$, while bands B, D, and F represent the corresponding singlet states, respectively.

The spectrum of $GeAu_8^-$ (Figure 4b) is much more complicated as compared to that of $SiAu_8^-$. The X band defines a VDE of 2.73 eV, much smaller than that of $SiAu_8^-$. The energy gap between the first (X) and second peaks (X′) does not look like a usual HOMO−LUMO gap, since the second band displays intensity similar to that of the first one. In addition, the spectral features between 4 and 5 eV in the spectrum of $GeAu_8^-$ are much more congested and complicated than any other species studied here, suggesting that there might be coexistence of

multiple isomers with nearly equal contributions to the observed spectrum. Indeed, a closer look reveals that parts of the spectral features in $GeAu_8^-$ (X, A, B) actually are very similar to the corresponding peaks in the spectrum of $SnAu_8^-$ (Figure 4c), suggesting that one of the isomers observed for $GeAu_8^-$ is similar to that of $SnAu_8^-$. Thus, bands X′, A′, and B′ should be due to a different isomer.

The spectrum of $SnAu_8^-$ is relatively simple with a large HOMO−LUMO gap of 1.37 eV (Figure 4c), suggesting a high stability of neutral $SnAu_8$ and possibly also high symmetry. The first VDE of $SnAu_8^-$ is 2.74 eV, which is very close to that of the X band in $GeAu_8^-$. The intense peak B with a shoulder (C) is again an indication of triplet−singlet splitting. The band A may also have a corresponding singlet part, which is likely buried in the intense band B.

5. Theoretical Results

The top-5 lowest-energy structures located for MAu_5^- to MAu_8^- (M = Si, Ge, Sn) are depicted in Figures S1−S4 in the Supporting Information, respectively, together with their simulated PES spectra. Tables 2−4 list the relative energies of the corresponding isomers at several levels of theory. The isomers are ranked on the basis of their relative energies at the PBE/TZP level (using ADF package) except a few leading isomers which are ranked at higher level theory (see table titles). The first VDEs of each species are calculated at the PBE/TZP level and compared with the experimental values in Tables 2−4, respectively.

5.1. MAu_5^-. For $SiAu_5^-$, DFT (ADF and G03), MP4(SDQ), and CCSD(T) computations all predict isomer 1 (C_{3v}) as the global minimum (Figure S1a in the Supporting Information), which can be viewed as a tetrahedral $SiAu_4$ bonded by another Au atom through a terminal gold atom. The MP2 calculations seem to prefer isomer 2 as the lowest energy, which is also of C_{3v} symmetry (Figure S1b in the Supporting Information). Two previously reported structures of neutral $SiAu_5$[26] are also checked and found to be higher-energy isomers for the anion $SiAu_5^-$ and disagree with the experiment. For $GeAu_5^-$, both PBE/TZT (ADF) and MP4(SDQ) calculations locate a C_s structure (isomer 1, Figure S1f in the Supporting Information) to be the global minimum, while MP2 calculation suggests isomer 1 is 0.064 eV higher than isomer 2. For $SnAu_5^-$, the lowest-energy structure is also the C_s structure (isomer 1, Figure S1k in the Supporting Information), similar to $GeAu_5^-$. The lowest-energy structures (at MP4 level) of $GeAu_5^-$ and $SnAu_5^-$ can be viewed as derived from the square-pyramidal $GeAu_4$ and $SnAu_4$,[25b] respectively, by attaching one more terminal Au atom. Notice that another structure related to the square-pyramidal $SnAu_4$, with one more bridging Au, is found to be 0.311 eV at PBE/TZP level and 0.21 eV at MP2 level for $SnAu_5^-$ (Figure S1o in the Supporting Information).

5.2. MAu_6^-. ADF and G03 DFT calculations, respectively, predict isomers 3 and 2 as the global minimum for $SiAu_6^-$. They are both three-dimensional and of C_s symmetries. Isomer 3 can be viewed as based on the tetrahedral $SiAu_4$ unit (Figure S2c in the Supporting Information). However, the higher-level MP4(SDQ) calculation reveals a C_1 structure (isomer 1, Figure S2a in the Supporting Information) as its ground state, which is *quasi-planar* and can be viewed as derived from isomer 3 of $SiAu_5^-$ by attaching one more bridging Au atom. For $GeAu_6^-$, all four levels of computations indicate that isomer 1 (C_1, Figure S2f in the Supporting Information) is the global minimum (Table 3). Like isomer 1 of $SiAu_6^-$, isomer 1 of $GeAu_6^-$ is also *quasi-planar* and can be viewed as derived from isomer 1 of $GeAu_5^-$. Isomer 2 (Figure S2g in the Supporting Information), which is an edge-bridged triangle with the Ge atom located at one apex, is found to be very close in energy (0.033 eV at MP4(SDQ)). For $SnAu_6^-$, two C_1 structures (isomers 1 and 2, Figure S2k,i in the Supporting Information) are found to be nearly degenerate in energy (Table 3). They are similar to isomer 2 and isomer 1 of $GeAu_6^-$, respectively. Another low-lying isomer 3 (C_s, Figure S2m in the Supporting Information), in which Sn atom is pentacoordinated, is also found close in energy to isomers 1 and 2 at DFT levels (Table 3). Notice that a similar structure as isomer 3 of $SnAu_6^-$ has been previously reported for $SiAu_6$,[26b] but we did not find it as low-lying isomer for $SiAu_6^-$.

5.3. MAu_7^-. For $SiAu_7^-$, while DFT (ADF) predicts a T_d $SiAu_4$-based structure (isomer 3, Figure S3c in the Supporting Information), all other levels of calculation locate a *quasi-planar* C_s structure (isomer 1, Figure S3a in the Supporting Information) as the global minimum (Table 4). This C_s isomer can be viewed as built upon isomer 1 of $SiAu_6^-$ by adding one Au atom to bond with the bridging gold and an apex gold atom. A similar structure has been reported for neutral $SiAu_7$.[26b] For $GeAu_7^-$, the lowest-energy structure found is isomer 1, which has the same structure as $SiAu_7^-$ (Figure S3f in the Supporting Information). For $SnAu_7^-$, two DFT methods show that isomers 1 and 2 are very close in energy, while MP2 and MP4(SDQ) clearly favor isomer 1 as the global minimum (Table 4), which has a similar *quasi-planar* C_s structure as that of $SiAu_7^-$ and $GeAu_7^-$. In isomer 2, the Sn atom is pentacoordinated.

5.4. MAu_8^-. The C_s isomer 1 (Figure S4a in the Supporting Information) is found as the lowest-energy structure for $SiAu_8^-$, and all other structures are substantially higher in energy (Table 5). It is a 3D structure containing a tetrahedral $SiAu_4$ unit. It can also be viewed as a dangling Au−Si unit sitting on the surface of a seven gold atom cluster, resembling the structural motif of the larger Si-doped gold cluster $SiAu_{16}^-$.[28] For $GeAu_8^-$, isomers 1 and 2 are nearly iso-energetic at DFT levels, while MP2 calculations predict isomer 1 as the global minimum. Isomers 1 and 2 are very similar; both can be viewed as evolved from the global minimum structure of $GeAu_7^-$ by adding one bridging Au atom at the bottom and some subsequent structural relaxation. In isomer 1 the dopant Ge atom is tetracoordinated, while in isomer 2 it is pentacoordinated (Figure S4f,g in the Supporting Information)). Note that isomer 3, which is 0.152 eV above isomer 1 at the PBE/TZP (ADF) level, can also be derived from the global minimum of $GeAu_7^-$ by adding a bridging Au atom at a side instead of at the bottom. For $SnAu_8^-$, isomer 1 with C_s symmetry is located as the global minimum. It is the same structure as isomer 2 of $GeAu_8^-$ but with a pentacoordinated Sn (Figure S4k in the Supporting Information).

6. Structure Assignments and Discussions

The well-resolved PES spectra allow a detailed comparison with the theoretical simulations, as shown in Figures S1−S4 in the Supporting Information, to assign the ground-state structures of the MAu_{5-8}^- (M = Si, Ge, Sn) clusters. The lowest-energy isomer whose simulated spectrum agrees best with the experiment is assigned as the primary structure for each of the clusters. For some species, minor isomers are also assigned on the basis of the experimental observations. The assigned structures of MAu_5^- to MAu_8^- and their simulated spectra are presented in Figures 1−4, respectively, where they are compared with the experimental spectra.

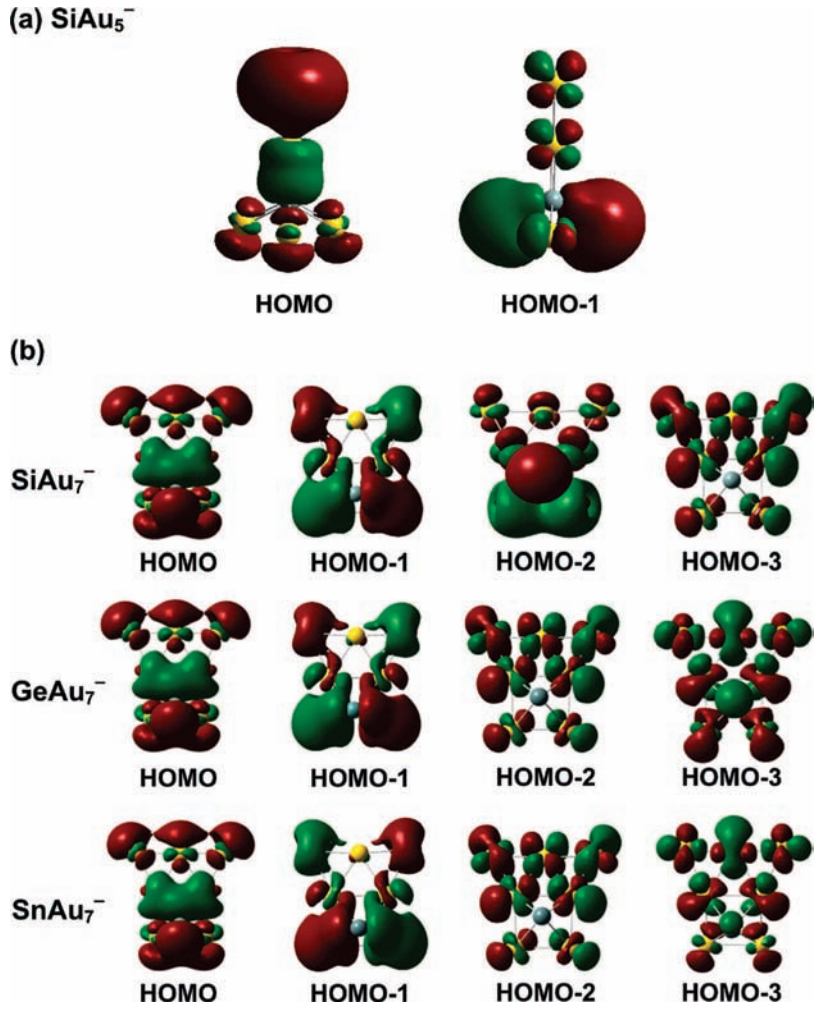

Figure 5. Selected frontier molecular orbitals of (a) $SiAu_5^-$ and (b) MAu_7^- (M = Si, Ge, Sn).

6.1. MAu_5^-. For $SiAu_5^-$, the lowest-energy isomer 1 gives a well-matched PES pattern as compared to that of the experiment. Specifically it gives congested features in between 4−5 eV and 5−6 eV, which can be qualitatively correlated with the broad features A and B in the experimental spectra, respectively (Figure 1d). Moreover, considering its likelihood of growing from the very stable T_d $SiAu_4$,[24a] as suggested by the similarities between its spectrum and that of $SiAu_4^-$, we assign isomer 1 (C_{3v}) as the most stable structure of $SiAu_5^-$. Molecular orbital analysis (Figure 5a) shows that the HOMO of $SiAu_5^-$ is primarily made up of the 6s atomic orbital of the terminal Au atom, while the HOMO−1 is nearly identical to the HOMO of neutral $SiAu_4$.[25b] This indicates that its electronic structure is not significantly altered as compared to that of $SiAu_4$ and the extra terminal Au atom in $SiAu_5^-$ provides a relatively localized orbital to accommodate the two extra electrons (relative to $SiAu_4$), consistent with the experimental observations.

For $GeAu_5^-$, the simulated PES spectrum of the global minimum structure, isomer 1 (C_s), agrees best with the experiment. Particularly, the first doublet features (X and A) are well reproduced in the simulation. All other structures should have negligible contribution to the PES spectrum. For $SnAu_5^-$, isomer 1 (C_s) is assigned as the primary structure which is similar to that of $GeAu_5^-$, consistent with their similar PES spectra. Isomer 5 of $SnAu_5^-$ gives a transition at ∼2.7 eV, and it is assigned as a minor isomer to account for the weak feature (X′) observed in its spectrum. Both isomers 1 and 5 can be viewed as derived from the square-pyramidal $SnAu_4$.[25b]

6.2. MAu_6^-. For $SiAu_6^-$, the top-3 isomers all appear to provide good match to the experimental PES spectra in terms of the first VDE and the HOMO−LUMO gap (Figure S2a−c in the Supporting Information). However, on the basis of the energy ordering at high-level MP4(SDQ) calculations (Table 3), as well as its similarity to $GeAu_6^-$ and $SnAu_6^-$ as suggested by the experimental observations, isomer 1 (C_1) is taken as the ground-state structure for $SiAu_6^-$.

For $GeAu_6^-$, the global-minimum isomer 1 gives the best match to the experimental PES spectrum (Figure S2g in the Supporting Information) and its VDE is also in good agreement with the observed value (Table 3). The nearly iso-energetic isomer 2 is assigned as a minor isomer, whose simulated PES spectrum well reproduces the weak feature (X′) observed in the experimental spectrum (Figure 2b,e). For $SnAu_6^-$, the nearly iso-energetic isomers 2 and 1 are assigned as the primary and secondary isomers contributing to the PES spectrum, respectively, similar to the case of $GeAu_6^-$. However, for $SnAu_6^-$, the experimental PES spectrum suggests that there is an additional minor isomer populated in the beam, which gives rise to the weak peak X″ at ∼2.30 eV. Indeed, isomer 3 is found to be only 0.032 eV above the global minimum (at PBE/TZP level) and its first VDE (2.33 eV) agrees very well with that of the band X″ (Figure 2f).

We would like to point out that band B in the experimental spectra, assigned to transitions to singlet final states of neutral MAu_6, could not be reproduced in the theoretical simulations (Figure 2), because the simulated PES spectra are basically plots of density of states, disregarding the detailed electronic configurations.

6.3. MAu_7^-. For MAu_7^- (M = Si, Ge, Sn), isomer 1 is universally assigned to each species. They all represent the global minimum at the ab initio levels, and their simulated PES spectra agree well with the experiment (Figure 3). For $SiAu_7^-$, the theoretical results show that the second band in the simulated PES spectrum (Figure 3d), which is apparently higher and broader than that of $GeAu_7^-$ and $SnAu_7^-$, indeed contains two transitions separated by 0.069 eV. This is in good agreement with the doublet features (A and B) in the experimental PES spectrum with a separation of 0.12 eV (Figure 3a), confirming the global minimum of isomer 1. For $GeAu_7^-$ and $SnAu_7^-$, isomer 2 also shows good agreement with the experiment. However, it is ruled out on the basis of its higher energy at MP2 and MP4(SDQ) levels, as well as the experimental evidence of the similarities among the three MAu_7^- clusters.

The first four molecular orbitals of MAu_7^- are plotted in Figure 5b. Interestingly, although MAu_7^- has very similar structures, their molecular orbitals show some differences in orders. Particularly, the HOMO−2 of $SiAu_7^-$, which is dominated by the Si atom, is very different from that of $GeAu_7^-$ and $SnAu_7^-$, which shows little contribution from the dopant atom. This well explains the appreciable difference observed in the VDE of the B band, which corresponds to detachment from HOMO−2, between $SiAu_7^-$ and $GeAu_7^-$/$SnAu_7^-$ (Figure 3 and Table 4), lending further support to the structure assignment for MAu_7^-.

6.4. MAu_8^-. For M = Si and Sn, clearly structure 1 is the primary isomer observed in the experiment. It is the lowest-energy structure by DFT calculations, and its simulated PES spectrum agrees very well with the experimental data except that transitions to singlet states could not be reproduced in the simulation (Figure 4d, f), similar to the case of MAu_6^-. For $GeAu_8^-$, isomers 1 and 2 are very similar in structure, as are their simulated PES spectra (Figure S4f,g in the Supporting Information). They both fit the experimental VDE well. Considering their very close energies (at DFT level; Table 5), it is possible that both isomers 1 and 2 of $GeAu_8^-$ are populated. As aforementioned, the complicated PES spectrum of $GeAu_8^-$ suggests that there should be at least one more isomer present to account for the features X′, A′, and B′. The next low-lying structure, isomer 3, seems to fit. As seen in Figure 4e, by assuming equal population of isomers 1, 2, and 3, the simulated PES spectra of the mixture acquire good agreement with the experimental data. However, we note that isomer 3 is >0.15 eV (PBE/TZP level) above the calculated global minimum. Usually it is rare to have such a high-energy isomer with large population in the experiment. One possibility is that the relative energy of isomer 3 for $GeAu_8^-$ may be somewhat overestimated by the current theoretical methods.

To summarize, the most intriguing finding in our structural study of MAu_{5-8}^- (M = Si, Ge, Sn) is the 3D ($SiAu_5^-$) → *quasi-planar* 2D ($SiAu_6^-$ and $SiAu_7^-$) → 3D ($SiAu_8^-$) structural evolution of the Si-doped clusters, which leads to a *structural convergence* for MAu_x^- (M = Si, Ge, Sn) at $x = 6, 7$. It reflects the competition between the strong tendency of forming tetrahedral bonding structures around the Si atom (M−Au interactions) and the strong tendency of forming planar structures for small anion gold clusters (Au−Au interactions). We have shown before that, because of the strong sp^3 hybridization of the Si atom, the structures of Si-doped gold clusters are usually dominated by the local tetrahedral $SiAu_4$ unit (e.g., in $SiAu_4^-$ [24a] and $SiAu_{16}^-$ [28]). The corresponding Ge- or Sn-doped gold clusters show different structural motif, reflecting its lower tendency of sp^3 hybridization in the doped clusters. Particularly, $GeAu_4^-$ and $SnAu_4^-$ do not have T_d structures as that of $SiAu_4^-$ but a square-pyramidal structure in which the dopant atom is located slightly above the plane of a square Au_4 unit.[25b] This structural behavior of MAu_4^- also correlates with the trend of M−Au bonding energy, which is ∼71.2, 68.1, and 66.2 kcal/mol, respectively, for M = Si, Ge, and Sn (computed at the CCSD(T)/SDD//MP2/SDD level of theory). Our results also show that, because of the high stability of tetrahedral $SiAu_4$, the structure of $SiAu_5^-$ is still T_d-based, in which the Si atom is tetrahedrally coordinated to four Au atoms to optimize the local Si−Au interactions. However, $SiAu_6^-$ and $SiAu_7^-$ show *quasi-planar* structures, in which the Si atom is also fourfold-coordinated but with a square-pyramidal local arrangement. This anomaly in structural evolution reflects that, as the cluster size increases, the Au−Au interactions become competitive and important in determining the cluster structures. The strong tendency of forming planar structures for Au_6^- and Au_7^- results in the *quasi-planar* structures of $SiAu_6^-$ and $SiAu_7^-$ in which the Au−Au interactions dominate. As the number of gold atoms further increases, the delicate balance between the above-mentioned two factors results in the convex structure for $SiAu_8^-$, which can be viewed as a Au−Si dangling unit bonded to a quasi-planar Au_7, reminiscent of the structure motif of $SiAu_{16}^-$.[28] On the other hand, the dopants Ge and Sn behave similarly in the doped clusters under study. The major isomers of $GeAu_{5-8}^-$ all have similar structures as the corresponding $SnAu_{5-8}^-$ clusters, and they can simply be viewed as evolved from the motif of square-pyramidal $GeAu_4^-$ and $SnAu_4^-$, respectively, by successive addition of Au atoms with subsequent structural relaxation.

7. Conclusions

In conclusion, we conducted a combined photoelectron spectroscopy and computational study on the structural evolution of doped gold anion clusters MAu_x^- (M = Si, Ge, Sn; x = 5−8). For $x = 5$, the $SiAu_5^-$ cluster was observed to have a tetrahedral-based 3D structure, while the primary isomers of $GeAu_5^-$ and $SnAu_5^-$ have quasi-planar structures based on a square-pyramid motif. For $x = 6$ and 7, all three doped clusters MAu_x^- (M = Si, Ge, Sn) exhibit similar *quasi-planar* structures. This unusual *structural convergence* reflects a subtle and delicate competition between Au−Au interactions and Au−M interactions in the MAu_x^- clusters. For $x = 8$, $SiAu_8^-$ again has a 3D structure and starts showing a Au−Si dangling unit, resembling that of the larger Si-doped gold cluster $SiAu_{16}^-$. It is reasonable to speculate that such a structural motif is kept through all the medium-sized $SiAu_x^-$ clusters with x = 8−16. In contrast, $GeAu_8^-$ and $SnAu_8^-$ still have quasi-planar structures. It would be interesting to locate the size at which the quasi-2D to 3D transition occurs in MAu_x^- (M = Ge, Sn). Research progress in this direction is underway.

Acknowledgment. The experimental work done in Washington was supported by the National Science Foundation (CHE-0749496) and was performed at the EMSL, a national scientific user facility sponsored by the DOE's Office of Biological and Environmental

Research and located at the Pacific Northwest National Laboratory, operated for DOE by Battelle. The theoretical work done in Nebraska was supported by grants from the National Science Foundation (CHE, CMMI, DMR/MRSEC), ARO, the Nebraska Research Initiative, and the UNL Research Computing Facility and Holland Supercomputing Center at University of Nebraska-Omaha. We thank Dr. Satya Bulusu for helpful discussions.

Supporting Information Available: Structures, simulated PES spectra, harmonic vibrational frequencies, corresponding IR intensities of low-lying isomers, and complete ref 35. This material is available free of charge via the Internet at http://pubs.acs.org.

JA810093T